Journal of Materials Science and Chemical Engineering, 2026, 14(11), 82-94
https://www.scirp.org/journal/msce
ISSN Online: 2327-6053
ISSN Print: 2327-6045

Thickness-Dependent Performance of PEDOT:PSS Hole-Transport-Layer Organic Photovoltaic Cells: A TCAD Study

Mouhamadou Sam[1*], Alioune Ngom[1], Fatma Sow[1], Ahmed Mohamed-Yahya[2], Mamadou Lamine Samb[1]

[1]Department of Physics and Chemistry, University Iba Der Thiam of Thiès, Thiès, Senegal
[2]Applied Research Unit for Renewable Energies, University of Nouakchott, Nouakchott, Mauritania
Email: *mouhamdou.sam@univ-thies.sn

How to cite this paper: Sam, M., Ngom, A., Sow, F., Mohamed-Yahya, A. and Samb, M.L. (2026) Thickness-Dependent Performance of PEDOT:PSS Hole-Transport-Layer Organic Photovoltaic Cells: A TCAD Study. *Journal of Materials Science and Chemical Engineering*, **14**, 82-94.
https://doi.org/10.4236/msce.2026.1411005

Received: August 26, 2026
Accepted: November 23, 2026
Published: November 26, 2026

Copyright © 2026 by author(s) and Scientific Research Publishing Inc.
This work is licensed under the Creative Commons Attribution International License (CC BY 4.0).
http://creativecommons.org/licenses/by/4.0/
Open Access

Abstract

This study uses Silvaco ATLAS to examine how the thickness of the PEDOT:PSS hole-transport layer affects an idealized ITO/PEDOT:PSS/organic/ZnO/Al photovoltaic device. The HTL thickness is varied from 1 to 100 nm over 37 simulation points, while the active-layer thickness (320 nm), ZnO thickness (10 nm), material parameters and doping concentrations are held fixed. Under the specified AM1.5 optical setup, the calculated short-circuit current density, fill factor and power conversion efficiency decrease as the HTL becomes thicker; the open-circuit voltage changes less and approaches a plateau. These findings describe the response of this parameter set and do not establish a general design rule. The continuum model treats the layers as homogeneous and does not resolve film coverage, pinholes, interface defects or tunneling. In particular, its 1 - 10 nm cases are idealized limits rather than predictions for fabricated films. No experimental J-V benchmark or mesh-convergence study is available, and the constant optical indices may overestimate photogeneration. The calculated efficiencies therefore should not be interpreted as validated device performance or as evidence of a fabrication optimum. Further experimental comparison and model diagnostics are needed to identify the origin and practical relevance of the calculated thickness trend. At larger thicknesses, the relative plateau in V_{oc} alongside continuing declines in J_{sc} and FF indicates that the modeled penalty is more evident under current extraction and near maximum-power operation. Terminal J-V curves alone cannot distinguish resistance, field redistribution, or interface recombination.

Keywords

Organic Photovoltaics, PEDOT:PSS, ZnO, Hole Transport Layer, Thickness

Dependence, Charge Transport, TCAD Simulation

1. Introduction

Organic photovoltaic (OPV) cells are a lightweight, mechanically flexible, and solution-processable alternative to rigid inorganic technologies, with a cost structure compatible with roll-to-roll printing [1]. Their efficiency, however, remains sensitive to details of the layer stack that go beyond the active layer itself. The earliest three-layer anode/active-layer/cathode architecture was superseded once Peumans, Bulović and Forrest demonstrated that inserting a thin exciton/carrier blocking layer between the active layer and each electrode sharply raised photon-harvesting efficiency at high optical intensity [2], a result Forrest later placed in the broader context of low-cost organic electronics [3]. Xue, Rand, Uchida and Forrest confirmed the mechanism in a CuPc:C_{60} interpenetrating structure, reporting a power conversion efficiency near 5% with a blocking layer present against 3.5% without one [4]. These blocking layers are now more commonly called transport layers: the hole transport layer (HTL) and electron transport layer (ETL), and the modern architecture anode/HTL/active layer/ETL/cathode is the de facto standard.

The HTL is not a purely passive contact. It must simultaneously extract holes efficiently, block electrons from reaching the anode, and avoid introducing excessive series resistance of its own. Its thickness is therefore a genuine design variable rather than a fixed constructional detail, and the literature on adjacent thin-film photovoltaic technologies shows this thickness dependence is rarely trivial [5] [6]. Numerical studies with SCAPS-1D on spiro-OMeTAD/PDINO-based bulk-heterojunction cells report that HTL thickness has a comparatively limited effect on efficiency once an adequate value is reached, with the active-layer thickness dominating the overall trend [7]. Experimentally, Ochiai *et al.* showed that both the composition and the thickness of a PEDOT:PSS HTL directly affect the PCE of PCDTBT:$PC_{71}BM$ devices, with conductivity-enhancing solvent treatments changing the optimal operating point [8]. More broadly, Scharber and Sariciftci's review of bulk-heterojunction efficiency limits underlines that interfacial and transport layers remain one of the more tunable levers separating laboratory devices from the Shockley-Queisser-adjacent ceiling for organic absorbers [9].

Recent interface-engineering studies reinforce this multi-function picture. Zhao *et al.* showed that conventional PEDOT:PSS commonly exhibits limited thickness tolerance, with favourable operation around 30 - 40 nm, whereas molecular modification that improves conductivity, interfacial dipoles and hole-selective extraction can preserve useful performance even at 170 nm [10]. Thus, HTL thickness has no universal optimum independent of material properties; the observed response emerges from the coupling of geometry with conductivity, energetic selectivity and interface quality. Solution-processed bilayer HTLs likewise demonstrate that

interface-layer design can control efficiency, process tolerance and operational stability [11].

Previous studies discuss series resistance as one contributor to fill-factor losses in organic solar cells [12]-[14]. In the present work, however, no independent resistance extraction or matched-resistor control is available. The literature therefore provides context for interpreting the thickness sweep but does not identify the cause of its simulated trend.

This paper examines how PEDOT:PSS thickness changes the terminal response of a fixed ITO/PEDOT:PSS/organic/ZnO/Al numerical device. The analysis is intended as a continuum-model sensitivity study. It distinguishes the calculated thickness dependence from physical mechanisms that would require internal carrier profiles, resistance extraction or experimental evidence. In particular, calculations in the 1 - 10 nm range are treated as idealized limiting cases and are not used to recommend an ultrathin film for fabrication.

2. Device Modelling

Incident radiation crosses the transparent ITO anode and the HTL before being absorbed in the organic active layer, where it generates excitons that dissociate into free carriers collected at the electrodes, following standard solar-cell device physics [15] [16]. The short-circuit current density collected from the three regions of the device (HTL, active layer, ETL) is:

$$J_{SC} = q\left[\int_0^{d_{HTL}} G_{HTL}(y)\eta_{HTL}(y)\mathrm{d}y + \int_{d_{HTL}}^{d_{HTL}+d_{org}} G_{org}(y)\eta_{org}(y)\mathrm{d}y + \int_{d_{HTL}+d_{org}}^{L} G_{ETL}(y)\eta_{ETL}(y)\mathrm{d}y\right] \quad (1)$$

where q is the elementary charge, d_{htl} and d_{etl} are the HTL and ETL thicknesses, $G_r(y)$ are the exciton generation rates, and $\eta_r(y)$ are the carrier collection probabilities in each region r. Because excitons are photogenerated only in the active layer ($G_{htl} = G_{etl} = 0$), Equation (1) reduces to a single integral over the active-layer generation rate, which follows the Beer-Lambert law:

$$G_{org}(y) = \alpha\Phi_0 \mathrm{e}^{-\alpha y} \quad (2)$$

with Φ_0 the incident photon flux and α the absorption coefficient. For a sufficiently thin absorbing layer, this is sometimes simplified using the thin-layer approximation:

$$\mathrm{e}^{-\alpha d} \approx 1 \ \left(\text{valid only where } \alpha d \ll 1\right) \quad (3)$$

This approximation is only strictly valid where $\alpha d \ll 1$, a condition that should be checked against the active-layer thickness and absorption coefficient used in the simulation rather than assumed from the layer being nominally "thin"; it is retained here as the interpretive framework behind the generation-rate term, while the reported J-V output itself comes from ATLAS's full drift-diffusion solution rather than from this simplified closed form. The resulting open-circuit voltage follows the standard diode relation:

$$V_{OC} = \frac{nkT}{q} \ln\left(1 + \frac{J_{SC}}{J_0}\right) \tag{4}$$

and the four extracted photovoltaic parameters combine into the power conversion efficiency:

$$\text{PCE} = \frac{V_{OC} \times J_{SC} \times \text{FF}}{P_{in}} \tag{5}$$

with P_{in} = 100 mW·cm^{-2} under AM1.5 illumination.

3. Numerical Methodology

The PEDOT:PSS HTL was uniformly p-type doped at $N_A = 1 \times 10^{17}$ cm^{-3}, while its thickness was varied from 1 to 100 nm. The ZnO ETL was uniformly n-type doped at $N_D = 1 \times 10^{17}$ cm^{-3}. Illumination was defined in ATLAS using the AM1.5 spectrum over the wavelength range 0.30 - 1.20 μm, sampled at 100 spectral points, with normal incidence ($\theta = 90^\circ$). An incident power density P_{in} = 100 mW·cm^{-2} was used for the calculation of PCE.

The device equations were solved within the drift-diffusion framework implemented in Silvaco ATLAS [17]. Shockley-Read-Hall (SRH) recombination [18] [19], field-dependent mobility and optical absorption/photogeneration were included. Illuminated J-V characteristics were calculated using a voltage increment of 0.01 V. J_{sc}, V_{oc}, the maximum-power point, FF and PCE were extracted for each HTL thickness. All material, contact, illumination and numerical parameters other than PEDOT:PSS thickness were kept unchanged throughout the sweep. Consequently, the simulations are used primarily as a controlled comparative study of thickness dependence; the calculated absolute photovoltaic outputs remain conditional on the optical and electrical assumptions of the model.

Photovoltaic outputs are reported to approximately three significant figures. This reporting convention avoids implying an accuracy unsupported by the model; it does not constitute an uncertainty estimate. Derived quantities were calculated before rounding.

The simulations represent each layer as continuous and homogeneous, with thickness-independent bulk parameters. No explicit film-coverage model, interface-defect population or tunneling treatment is included in the reported analysis. Accordingly, the 1 - 10 nm interval is retained as an idealized continuum extrapolation. No universal physical validity threshold is assumed at 10 nm.

No experimental J-V calibration is available for the present device. Furthermore, the voltage increment used to sample the J-V curves does not, by itself, demonstrate mesh independence or numerical convergence.

4. Device Structure

The simulated ITO/PEDOT:PSS/organic/ZnO/Al stack is shown in **Figure 1**. The electrical and transport parameters used in ATLAS are summarized in **Table 1**.

Table 1. Electrical and transport parameters used in the ATLAS simulations.

Parameter	Symbol	Active layer	PEDOT:PSS (HTL)	ZnO (ETL)
Band gap	E_g	2.1 eV	1.3 eV	3.2 eV
Electron affinity	χ	2.8 eV	3.6 eV	4.26 eV
Relative permittivity	ε_r	4	3.5	9
Effective CB density of states	N_C	2.5×10^{19} cm^{-3}	1×10^{21} cm^{-3}	2×10^{18} cm^{-3}
Effective VB density of states	N_V	2.5×10^{19} cm^{-3}	1×10^{21} cm^{-3}	1.8×10^{19} cm^{-3}
Electron mobility	μ_n	1×10^{-3} cm^2·V^{-1}·s^{-1}	1×10^{-4} cm^2·V^{-1}·s^{-1}	200 cm^2·V^{-1}·s^{-1}
Hole mobility	μ_p	1×10^{-3} cm^2·V^{-1}·s^{-1}	2×10^{-5} cm^2·V^{-1}·s^{-1}	5 cm^2·V^{-1}·s^{-1}
Electron lifetime	τ_n	1×10^{-6} s	—	—
Hole lifetime	τ_p	1×10^{-6} s	—	—
Doping concentration	N	—	1×10^{17} cm^{-3} (p-type)	1×10^{17} cm^{-3} (n-type)

Note: PEDOT:PSS and ZnO parameter values were adopted from Ref. [20].

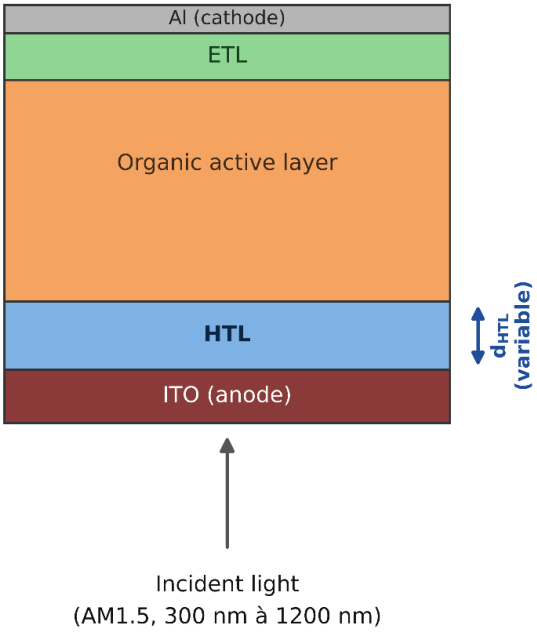

Figure 1. Schematic of the simulated ITO/PEDOT:PSS/organic/ZnO/Al device, showing the illumination direction and variable PEDOT:PSS HTL thickness. The active-layer and ZnO thicknesses are fixed at 320 and 10 nm, respectively.

The active-layer optical model uses constant effective refractive-index values $n = 3$ and $k = 1$ over the simulated spectral window. These values are retained unchanged for all PEDOT:PSS thicknesses to preserve a common optical baseline for the comparative sweep. They do not constitute a wavelength-resolved experimental optical spectrum and do not explicitly impose the absorption edge associated with $E_g = 2.1$ eV. Accordingly, the optical model can overestimate the absolute photogeneration/current if sub-bandgap wavelengths contribute through the constant-k approximation. Holding these optical inputs fixed across the thickness sweep does not eliminate their influence on the calculated transport losses. Field-

dependent mobility is included for the active layer with $\Delta E_n = 0.05$ eV, $\Delta E_p = 0.02$ eV and $\beta_n = \beta_p = 1.5 \times 10^{-4}$, as implemented in the simulation script. These transport quantities are likewise kept fixed for all HTL thicknesses.

Adopting parameters from another device simulation does not transfer that study's experimental calibration to the present stack.

5. Results and Discussion

5.1. J-V Characteristics

Figure 2 compares representative simulated J-V curves. Increasing HTL thickness lowers the delivered current and reduces the maximum-power region, while the voltage intercept changes less strongly. Selected photovoltaic parameters are summarized in Table 2.

The curves in the 1 - 10 nm interval are retained to document the numerical sweep, but they do not establish the performance of fabricated ultrathin PEDOT:PSS films. Terminal J-V characteristics alone cannot separate the contributions of resistive transport, electrostatic redistribution and recombination.

Table 2. Selected simulated photovoltaic parameters, rounded to approximately three significant figures.

HTL thickness (nm)	J_{sc} (mA·cm^{-2})	V_{oc} (V)	FF (%)	Model PCE (%)
1*	34.3	1.67	33.6	19.3
20	33.0	1.62	30.9	16.5
50	30.5	1.61	27.8	13.6
100	25.0	1.61	25.5	10.2

The 1 nm row represents an idealized limiting calculation. The entries are simulated outputs, not measured device performance. Rounding does not quantify uncertainty; derived quantities were calculated before rounding.

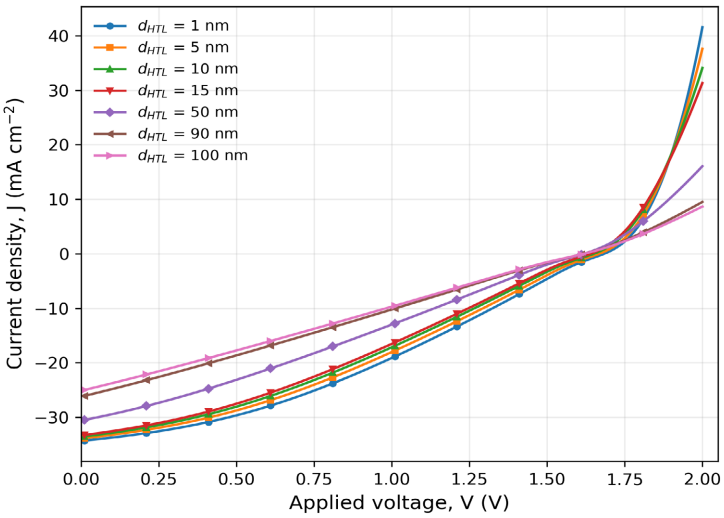

Figure 2. Simulated illuminated J-V characteristics for selected PEDOT:PSS HTL thicknesses from 1 to 100 nm. Curves in the 1 - 10 nm range are idealized continuum-model limits.

5.2. Effect of HTL Thickness on J_{sc}

Figure 3 shows a decrease in calculated J_{sc} throughout the sampled thickness range. The decline continues at larger thicknesses, unlike the voltage response discussed below. Selected values are provided in Table 2.

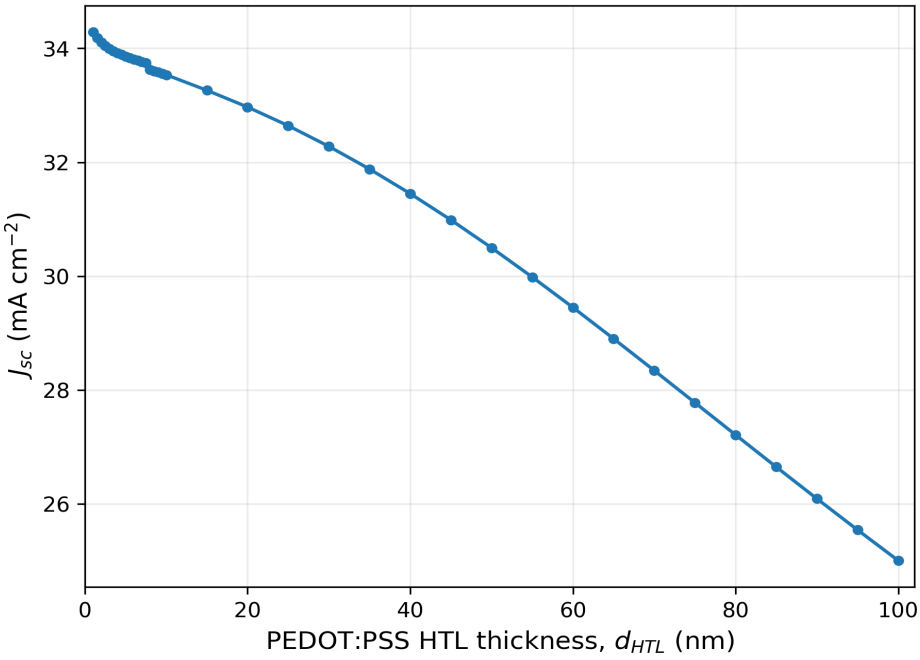

Figure 3. Simulated short-circuit current density, J_{sc}, as a function of PEDOT:PSS HTL thickness from 1 to 100 nm. Values in the 1 - 10 nm range are idealized continuum-model limits.

A longer hole-transport path at fixed mobility and doping is consistent with a collection penalty. However, spatial carrier and recombination profiles are needed to determine how that penalty develops within the device. The constant optical indices also influence photogeneration and the operating conditions under which transport losses occur. The calculated J_{sc} dependence therefore remains conditional on the specified optical and electrical parameter set.

5.3. Effect of HTL Thickness on V_{oc}

Figure 4 shows a voltage response that tends toward saturation as HTL thickness increases. The change is concentrated toward the lower part of the simulated range. By approximately 50 nm, V_{oc} is close to its large-thickness plateau, although current collection continues to decline.

A standalone series resistor added to an otherwise unchanged ideal diode would not change V_{oc} because the terminal current is zero at open circuit. Changing the thickness of a layer within a drift-diffusion device can also alter its internal electrostatic and recombination solution. The observed voltage change is compatible with such coupling, but the terminal characteristics do not identify the responsible contribution.

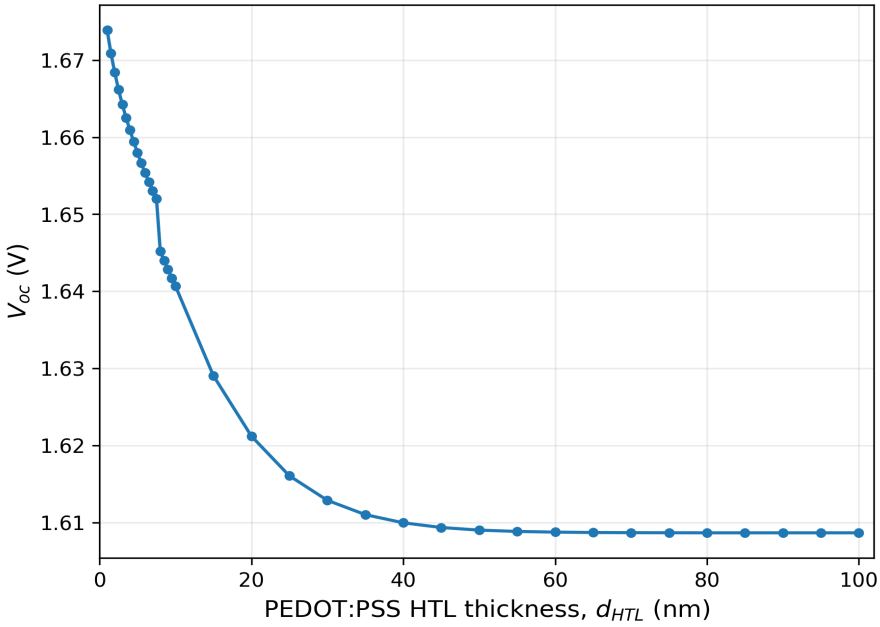

Figure 4. Simulated open-circuit voltage, V_{oc}, as a function of PEDOT:PSS HTL thickness from 1 to 100 nm. Values in the 1 - 10 nm range are idealized continuum-model limits.

5.4. Effect of HTL Thickness on Fill Factor

Figure 5 shows a continuing decline in FF as the HTL becomes thicker. Unlike V_{oc}, FF does not reach a clear plateau over the plotted interval. This indicates a progressively less favorable current-voltage balance near maximum power within the specified model.

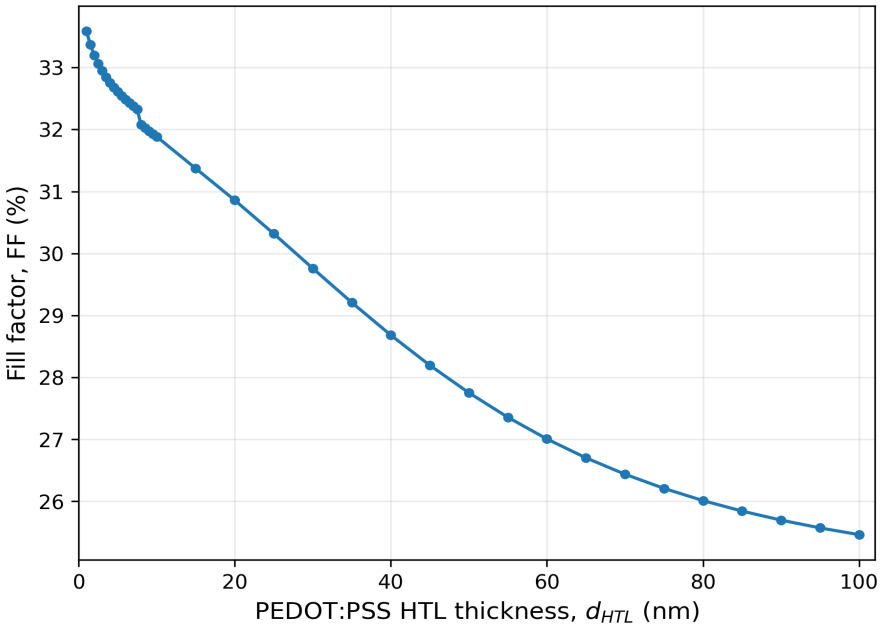

Figure 5. Simulated fill factor, FF, as a function of PEDOT:PSS HTL thickness from 1 to 100 nm. Values in the 1 - 10 nm range are idealized continuum-model limits.

At fixed conductivity, a thicker homogeneous transport layer is expected to introduce a larger geometrical resistance. The direction of the calculated FF trend is therefore consistent with an anticipated transport penalty. Neither a thickness-resolved extraction of series resistance nor a control calculation with a matched lumped resistor is available to establish how much of the response this explanation accounts for.

The different thickness sensitivities of FF and V_{oc} show that maximum-power operation continues to deteriorate after the voltage has nearly stabilized. This observation describes the numerical response but does not quantify separate transport and recombination losses.

5.5. Effect of HTL Thickness on PCE

Figure 6 presents the calculated PCE as a function of HTL thickness. The largest calculated efficiency occurs at the lower boundary of the thickness sweep. Because this boundary lies in the unvalidated ultrathin regime, it cannot be identified as a practical optimum or a recommended thickness for fabrication. The reported efficiencies also remain conditional on the optical model and the input-power normalization.

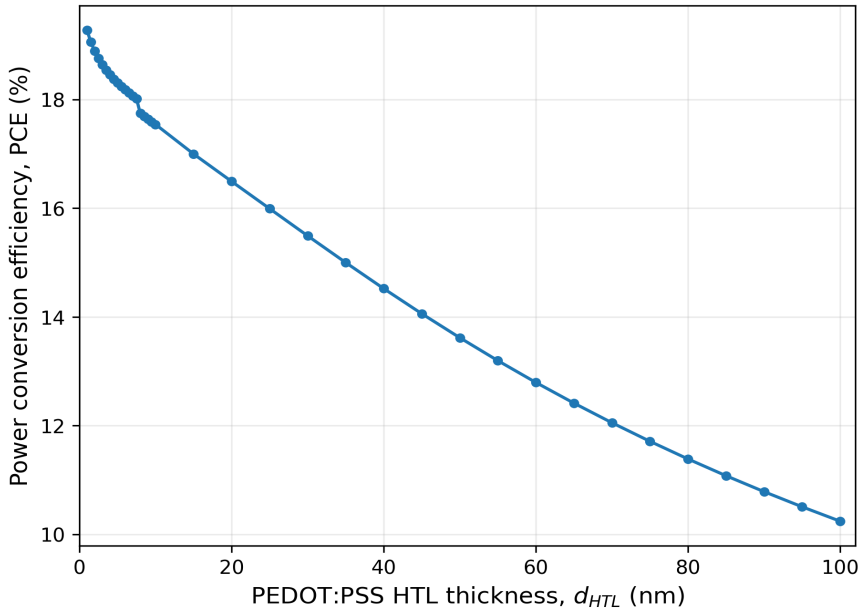

Figure 6. Simulated power conversion efficiency, PCE, as a function of PEDOT:PSS HTL thickness from 1 to 100 nm, using the stated reference input power. Values in the 1 - 10 nm range are idealized continuum-model limits and are not validated predictions for fabricated films.

5.6. Literature-Supported Interpretation of the Thickness Dependence

The calculation documents the thickness response of one specified parameter set. A monotonic decrease is compatible with the expected resistance penalty of thick-

ening a low-conductivity transport layer; it does not, by itself, demonstrate a new loss mechanism.

The different responses of V_{oc}, J_{sc} and FF indicate that the terminal characteristics do not evolve identically with thickness. Internal electric-field, carrier-density and recombination profiles, together with resistance-control calculations, would help determine the origin of these differences.

Experimental thickness optimization also involves film coverage, morphology and processing-dependent interface quality. These factors are absent from the present homogeneous-layer description. The model therefore does not reproduce the full experimental trade-off between adequate coverage at small thickness and transport losses at larger thickness. Literature comparisons provide context but do not constitute validation of the simulated J-V curves.

6. Model Limitations

The model assumes continuous, homogeneous layers with thickness-independent bulk parameters. Film coverage, pinholes, roughness and processing-dependent morphology are not represented. Consequently, the calculations at 1 - 10 nm are interpreted as idealized continuum limits and are excluded from claims about attainable ultrathin-film performance or fabrication optima. The study does not establish a universal thickness above which the continuum approximation becomes experimentally valid.

Interface-defect densities, their capture kinetics and tunneling processes are not explicitly resolved. Bulk Shockley-Read-Hall lifetimes do not substitute for these mechanisms. The available terminal J-V data also do not provide an independent decomposition of resistive and recombination losses.

The constant active-layer optical indices do not enforce a measured absorption edge and may produce excessive sub-bandgap absorption. This can affect absolute photogeneration, J_{sc} and PCE, as well as their sensitivity to transport parameters. The quoted efficiencies use a reference input-power density of 100 mW·cm^{-2}. The spectral interval of 0.30 - 1.20 μm and its normalization must be distinguished from a calculation covering the complete AM1.5 spectrum.

Finally, the model has not been benchmarked against experimental J-V curves for a device with matching materials and geometry. A mesh-refinement study and parameter-uncertainty analysis are also unavailable. Experimental benchmarking, wavelength-dependent optical inputs, appropriate interface models and convergence tests are required before the calculated values can be used as quantitative device-design predictions.

7. Conclusion

This study provides a controlled TCAD assessment of PEDOT:PSS HTL thickness in an ITO/PEDOT:PSS/organic/ZnO/Al photovoltaic device using literature-based transport parameters. Across the simulated thickness range, increasing the HTL thickness reduces the calculated short-circuit current density, fill factor and power

conversion efficiency, while the open-circuit voltage approaches a plateau. This contrast shows that, within the specified parameter set, thickness sensitivity is expressed most clearly during current collection and maximum-power operation. The study therefore establishes a comparative numerical baseline and identifies the device responses that warrant further investigation; it does not establish a universal thickness optimum or isolate a unique loss mechanism. In particular, the highest calculated efficiency at the 1 nm lower boundary is a model endpoint, not a fabrication recommendation. Experimental benchmarking, refined optical and interface descriptions, and convergence studies are needed before the results can support quantitative device-design guidance.

Acknowledgements

The authors thank Université Iba Der Thiam de Thiès (UIDT) for its financial support for the publication of this article through its Performance Contract (CDP).

Author Contributions

M.S.: conceptualization, simulation, formal analysis, and writing—original draft. A.N. and F.S.: supervision, project administration, validation, and writing—review. A.M.Y. and M.L.S.: methodology, formal analysis, and writing—review. All authors reviewed and approved the final manuscript.

Conflicts of Interest

The authors declare no conflicts of interest regarding the publication of this paper.

References

[1] Li, G., Zhu, R. and Yang, Y. (2012) Polymer Solar Cells. *Nature Photonics*, **6**, 153-161. https://doi.org/10.1038/nphoton.2012.11

[2] Peumans, P., Bulović, V. and Forrest, S.R. (2000) Efficient Photon Harvesting at High Optical Intensities in Ultrathin Organic Double-Heterostructure Photovoltaic Diodes. *Applied Physics Letters*, **76**, 2650-2652. https://doi.org/10.1063/1.126433

[3] Forrest, S.R. (2004) The Path to Ubiquitous and Low-Cost Organic Electronic Appliances on Plastic. *Nature*, **428**, 911-918. https://doi.org/10.1038/nature02498

[4] Xue, J., Rand, B., Uchida, S. and Forrest, S. (2005) A Hybrid Planar-Mixed Molecular Heterojunction Photovoltaic Cell. *Advanced Materials*, **17**, 66-71. https://doi.org/10.1002/adma.200400617

[5] Kirchartz, T. and Rau, U. (2018) What Makes a Good Solar Cell? *Advanced Energy Materials*, **8**, Article 1703385. https://doi.org/10.1002/aenm.201703385

[6] Hoppe, H. and Sariciftci, N.S. (2004) Organic Solar Cells: An Overview. *Journal of Materials Research*, **19**, 1924-1945. https://doi.org/10.1557/jmr.2004.0252

[7] Khan, M.R. and Jarząbek, B. (2023) Optimization and Efficiency Enhancement of Modified Polymer Solar Cells. *Polymers*, **15**, Article 3674. https://doi.org/10.3390/polym15183674

[8] Ochiai, S., Kumar, P., Santhakumar, K. and Shin, P. (2013) Examining the Effect of

Additives and Thicknesses of Hole Transport Layer for Efficient Organic Solar Cell Devices. *Electronic Materials Letters*, **9**, 399-403. https://doi.org/10.1007/s13391-013-0013-5

[9] Scharber, M.C. and Sariciftci, N.S. (2013) Efficiency of Bulk-Heterojunction Organic Solar Cells. *Progress in Polymer Science*, **38**, 1929-1940. https://doi.org/10.1016/j.progpolymsci.2013.05.001

[10] Zhao, B., Huang, X., Chung, S., Zhang, M., Zhong, Y., Liang, A., *et al.* (2025) Hole-selective-Molecule Doping Improves the Layer Thickness Tolerance of PEDOT:PSS for Efficient Organic Solar Cells. *eScience*, **5**, Article 100305. https://doi.org/10.1016/j.esci.2024.100305

[11] Xu, J., Heumüller, T., Le Corre, V.M., Barabash, A., Félix, R., Frisch, J., *et al.* (2024) A Polymer Bilayer Hole Transporting Layer Architecture for High-Efficiency and Stable Organic Solar Cells. *Joule*, **8**, 2570-2584. https://doi.org/10.1016/j.joule.2024.06.013

[12] Honsberg, C. and Bowden, S. (n.d.) Series Resistance. https://www.pveducation.org/pvcdrom/solar-cell-operation/series-resistance

[13] Saladina, M. and Deibel, C. (2025) Transport Resistance Strikes Back: Unveiling Its Impact on Fill Factor Losses in Organic Solar Cells. *Reports on Progress in Physics*, **88**, Article 038001. https://doi.org/10.1088/1361-6633/adb20c

[14] These, A., Koster, L.J.A., Brabec, C.J. and Le Corre, V.M. (2024) Beginner's Guide to Visual Analysis of Perovskite and Organic Solar Cell Current Density-Voltage Characteristics. *Advanced Energy Materials*, **14**, Article 2400055. https://doi.org/10.1002/aenm.202400055

[15] Nelson, J. (2003) The Physics of Solar Cells. Imperial College Press. https://doi.org/10.1142/p276

[16] Würfel, P. and Würfel, U. (2016) Physics of Solar Cells: From Basic Principles to Advanced Concepts. 3rd Edition, Wiley-VCH.

[17] Silvaco Inc. (2016) ATLAS User's Manual: Device Simulation Software. Silvaco International.

[18] Shockley, W. and Read, W.T. (1952) Statistics of the Recombinations of Holes and Electrons. *Physical Review*, **87**, 835-842. https://doi.org/10.1103/physrev.87.835

[19] Hall, R.N. (1952) Electron-Hole Recombination in Germanium. *Physical Review*, **87**, 387-387. https://doi.org/10.1103/physrev.87.387

[20] Okil, M., Shaker, A., Salah, M.M., Abdolkader, T.M. and Ahmed, I.S. (2023) Investigation of Polymer/Si Thin Film Tandem Solar Cell Using TCAD Numerical Simulation. *Polymers*, **15**, Article 2049. https://doi.org/10.3390/polym15092049

List of Abbreviations

AM1.5	Air Mass 1.5 solar spectrum
ATLAS	Device simulation module of Silvaco TCAD
CB	Conduction band
EQE	External quantum efficiency
ETL	Electron transport layer
FF	Fill factor
HTL	Hole transport layer
ITO	Indium tin oxide
J_{sc}	Short-circuit current density
OPV	Organic photovoltaic
PCE	Power conversion efficiency
PEDOT:PSS	Poly(3,4-ethylenedioxythiophene):poly(styrene sulfonate)
SCAPS-1D	Solar Cell Capacitance Simulator in one dimension
SRH	Shockley-Read-Hall
TCAD	Technology Computer-Aided Design
VB	Valence band
V_{oc}	Open-circuit voltage
ZnO	Zinc oxide